

Decadal (2011–2020) stratospheric aerosol variability observed by lidar over Saga, Japan

Osamu Uchino^{*1,2}, Tetsu Sakai¹, Isamu Morino², Tomohiro Nagai¹,
Hiroshi Okumura³, Yoshitaka Jin², Atsushi Ugajin², Tomoaki Nishizawa²,
Atsushi Shimizu², Tsuneo Matsunaga², and Kohei Arai³

¹*Meteorological Research Institute, 1-1 Nagamine, Tsukuba, Ibaraki 305-0052, Japan*

²*National Institute for Environmental Studies, 16-2 Onogawa, Tsukuba, Ibaraki 305-8506, Japan*

³*Saga University, 1 Honjou, Saga, Saga 840-8502, Japan*

(Received July 20, 2023; revised October 2, 2023; accepted October 11, 2023)

Lidar observations at the wavelength of 532 nm during 2011–2020 in Saga, Japan, revealed that stratospheric aerosols increased after the eruptions of Nabro volcano in Eritrea on 12 June 2011 and Raikoke volcano in the central Kuril Islands on 22 June 2019. Maximum values of the backscattering ratio and the integrated backscattering coefficient of stratospheric aerosols from tropopause altitude to 33 km after the Nabro eruption were 3.70 at 18.22 km on 23 June 2011 and $3.65 \times 10^{-4} \text{ sr}^{-1}$ on 25 July 2011, respectively; those after the Raikoke eruption were 1.89 at 17.47 km on 8 August 2019 and $3.01 \times 10^{-4} \text{ sr}^{-1}$ on 1 November 2019, respectively. Assuming a lidar ratio of 50 sr at 532 nm, the maximum stratospheric aerosol optical depth over Saga during the ten-year period from 2011 to 2020 was estimated to be 0.018 on 25 July 2011.

Stratospheric smoke particles from the Canadian forest fires in August 2017 were also detected. The degree of depolarization of smoke particles was about 0.1–0.18, and this value persisted for a long period of time, from 31 August 2017 to 22 February 22, 2018. These lidar data are useful for investigating the effects of stratospheric aerosols on climate and the ozone layer.

Key Words: Lidar, Stratospheric Aerosol, Volcanic eruption, Smoke

1. Introduction

Monitoring of the stratospheric aerosol layer is important because stratospheric aerosols affect the climate through radiative processes and the ozone layer through heterogeneous chemical reactions at the aerosol surface.^{1,2)} In addition, it is useful to investigate the stratospheric aerosols in the column-averaged dry air mole fractions of CO₂ and CH₄ (XCO₂ and XCH₄), products of the Greenhouse gases Observing SATellite (GOSAT).³⁾ As stratospheric aerosols with an optical thickness of 0.01 have been found to have an effect on XCO₂ at high latitudes in the Southern Hemisphere winter derived from the Orbiting Carbon Observatory-2 (OCO-2) satellite, a Gaussian stratospheric aerosol profile was introduced to improve the retrieval algorithm of OCO-2.⁴⁾

In 2008, the National Institute for Environmental Studies (NIES), Japan, in cooperation with the Meteorological Research Institute, Japan, developed a Mie-scattering lidar system to evaluate the influence of tropospheric and stratospheric aerosols and clouds on the GOSAT product with Total Carbon Column Observing Network Fourier Transform Spectrometer (TCCON FTS) and skyradiometer.³⁾ The Mie-scattering lidar system uses two wavelengths of the Nd:YAG laser (1064 nm and 532 nm) and can also observe the depolarization ratio at 532 nm. Using this lidar, we observed an increase in stratospheric aerosols caused by the Mt. Sarychev (48.08°N, 153.23°E) volcanic eruption on 12 June 2009.⁵⁾ To validate the tropospheric ozone data derived from the GOSAT thermal infrared spectra, a tropospheric

ozone differential absorption lidar (DIAL) system was developed at NIES from 2009 to 2010 and installed on a container together with the Mie-scattering lidar. In March 2011, the container containing the lidar systems was moved from NIES in Tsukuba to Saga University, Japan (33.24°N, 130.29°E), about 950 km to the southwest, after which we started lidar observations. We have previously reported several observation and analysis results obtained using the Mie-scattering lidar and the ozone DIAL,^{5,6)} and here we report on the stratospheric aerosol layer variations during 2011–2020 observed using the Mie-scattering lidar. First, the lidar system and data analysis method are described; next, the lidar observation results of stratospheric aerosols for 2011–2020 are presented; finally, the negative radiative forcing due to the increase in stratospheric aerosols after the 2011 Nabro and 2019 Raikoke volcanic eruptions is discussed.

2. Lidar system and data analysis

The laser output energy used to observe stratospheric aerosols at a wavelength of 532 nm was 130 mJ per pulse with a repetition rate of 10 Hz. The transmitted laser beam divergence was 0.2 mrad using a beam expander with a magnification factor of 5. The receiving telescope was a Schmidt-Cassegrain type with an aperture of 30.5 cm and a receiving field of view of 1.0 mrad. Three photomultiplier tubes (PMTs, R3234–01) were used as detectors, two to detect the parallel (P) component of the same polarization as the laser and one for the perpendicular (S) component. For signal processing, a 12-bit AD conversion and photon counting system (TR 20–160) was used.⁵⁾

The backscattering ratio (*BSR*) is defined as

$$BSR = \frac{BR + BA}{BR}, \quad (1)$$

where *BR* and *BA* are the molecular and particle backscattering coefficients, respectively. Previously, radiosonde data at Fukuoka were used to calculate *BR*, but since radiosondes sometimes do not reach more than 30 km, JRA-55 reanalysis data⁷⁾ were used instead to calculate *BR* and tropopause altitude. Because the wavelength of 532 nm is subject to ozone absorption, monthly average values for Kagoshima (31.55°N, 130.55°E) were used as the ozone model.⁸⁾ The lidar ratio *S* (the ratio of particle extinction to backscattering coefficient) was assumed to be 50 sr in this analysis.⁹⁾ The lidar backscatter signal was normalized to *BSR* = 1.02 (i.e., aerosol backscattering coefficient (*BA*) is 2% of the molecular backscattering coefficient (*BR*)) at 32–37 km altitude based on studies using satellite-borne stratospheric aerosol measurements.^{10–12)} We derived backscattering ratio profiles with an inversion method.¹³⁾ The vertical and time resolution of the raw lidar data were 7.5 m and 1 min, respectively. To improve the signal-to-noise ratio, lidar data were accumulated over an altitude of 150 m and temporally overnight. The time accumulation depended on the season because the sunrise and sunset were different depending on the season.

We obtained the integrated backscattering coefficient by summing up *BA* from the tropopause altitude to an altitude of 33 km. When cirrus clouds were present above the tropopause, we set the lower limit of the integration to just above the altitude of the cirrus clouds.

In this paper, the total linear depolarization ratio (*TDR*) is defined as

$$TDR = \frac{S}{P}, \quad (2)$$

where *P* and *S* are the parallel and perpendicular components of the backscattered signals, respectively. The total linear depolarization ratio δ so far⁵⁾ is

$$\delta = \frac{S}{P + S}. \quad (3)$$

The relationship between *TDR* and δ is as follows

$$TDR = \frac{\delta}{1 - \delta}. \quad (4)$$

Therefore, *TDR* is larger than δ .

The particle depolarization ratio *PDR* is calculated by

$$PDR = \frac{(1 + TDRm)TDR \cdot BSR - (1 + TDR)TDRm}{(1 + TDRm)BSR - (1 + TDR)}, \quad (5)$$

where $TDRm$ is the linear depolarization ratio of air molecules.¹⁴⁾ We used $TDRm = 3.66 \times 10^{-3}$.¹⁵⁾

3. Lidar observation results

During 2011–2020 over Saga, stratospheric aerosols increased mainly as the results of two volcanic eruptions, Nabro and Raikoke; in addition, smoke particles from large forest fires in Canada were detected in the stratosphere. In this section we discuss these lidar observational results. The lidar observation site (Saga) and the locations of the volcanoes (Nabro and Raikoke) and pyrocumulonimbus (pyroCbs) that contributed to the increase in stratospheric aerosols are shown in Fig. 1.

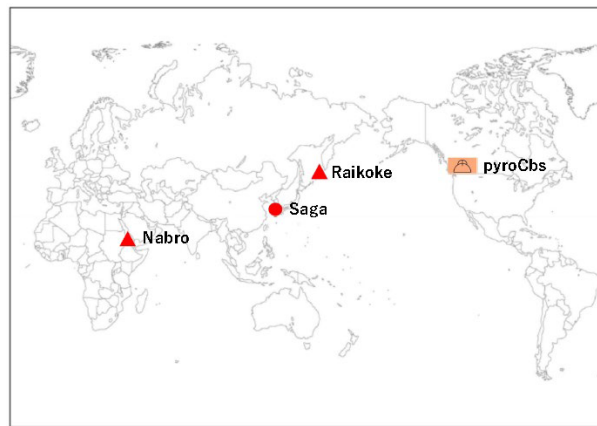


Fig. 1 Lidar observation site (Saga) and the locations of volcanoes (Nabro and Raikoke) and pyrocumulonimbus (pyroCbs).

3.1. Stratospheric aerosol increase due to the June 2011 eruption of Nabro volcano

Nabro volcano (13.37°N, 41.70°E) in Eritrea erupted on 12 June 2011. The total mass of SO_2 produced by the eruption was estimated to be 1.5 Tg.¹⁶⁾ Figure 2 shows vertical profiles of the aerosol backscattering ratio (BSR), total depolarization ratio (TDR), and particle depolarization ratio (PDR) at 532 nm over Saga. New aerosol layers with double peaks were observed on 23 June 2011, about 11 days after the eruption. The peak values of BSR were 2.25 and 3.70 at altitudes of 17.17 km and 18.22 km, respectively. The values of PDR were 0–0.016 at 17.2–18.2 km. Aerosols were probably composed of spherical particles because PDR was very small; however, some non-spherical particles were seen in the lower regions of the layers on 29 August 2011, and PDR was 0.03 at 16.4 km. An increase in stratospheric aerosols after the 2011 Nabro eruption was also confirmed by lidar observations at Tsukuba (36.1°N, 140.1°E).¹⁷⁾

3.2. Increase in stratospheric aerosols from the Raikoke volcanic eruption in June 2019

The Raikoke volcano (48.29°N, 153.25°E) in the central Kuril Islands erupted on 22 June 2019. The SO_2 injected into the upper troposphere and lower stratosphere by the Raikoke eruption was estimated to be 2.1 ± 0.2 Tg (larger than the initial estimate of 1.5 ± 0.2 Tg from earlier studies),^{18, 19)} and 40.5% (0.85 Tg) of the total SO_2 mass was injected into the lower stratosphere.²⁰⁾ Following the Raikoke eruption, stratospheric aerosol optical depth ($sAOD$) values increased in the whole Northern Hemisphere.²¹⁾

Vaughan et al.²²⁾ detected a thin layer at an altitude of 14 km late on 3 July, with the first detection of the main aerosol cloud on 13 July by a Raman lidar system based at the Capel Dewi Atmospheric Observatory, UK (52.4°N, 4.1°W). The Mauna Loa lidar first observed a 1-km-thick aerosol layer at an altitude of 26 km on September 24 after the Raikoke eruption.²³⁾

At Saga, stratospheric aerosols increased on 8 August 2019 (Fig. 3). The maximum value of BSR was 1.89 at 17.47

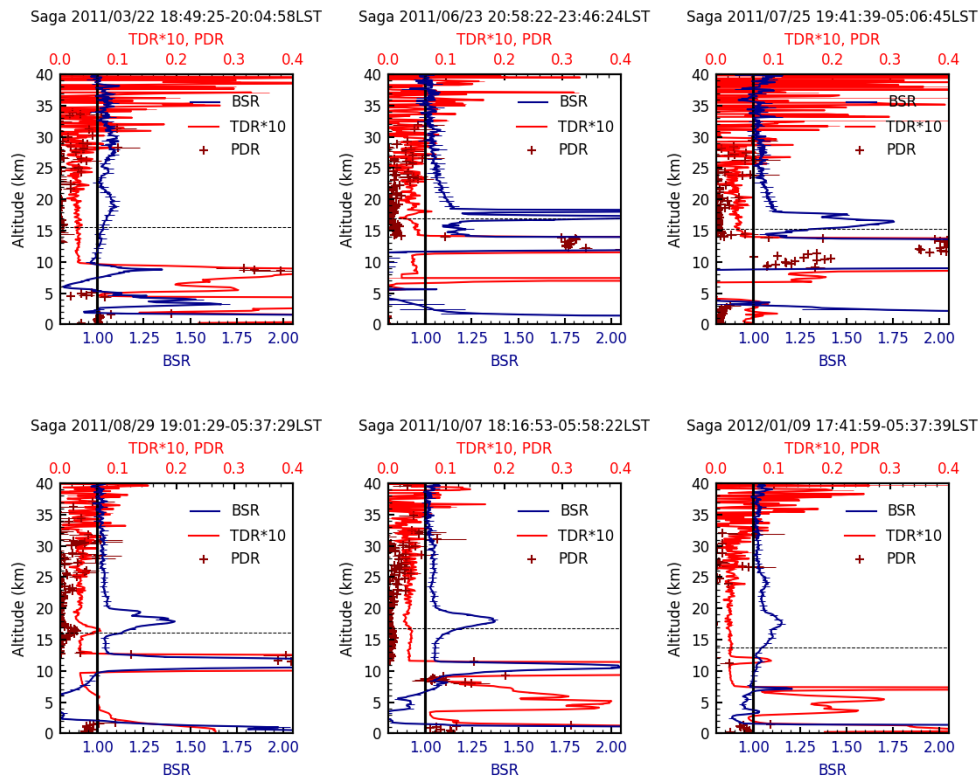


Fig. 2 Vertical profiles of aerosol backscattering ratio (*BSR*), total depolarization ratio (*TDR*), and particle depolarization ratio (*PDR*) at 532 nm over Saga, Japan, before and after the Nabro volcanic eruption in June 2011. LST stands for local standard time. The horizontal dotted lines show the mean tropopause altitudes.

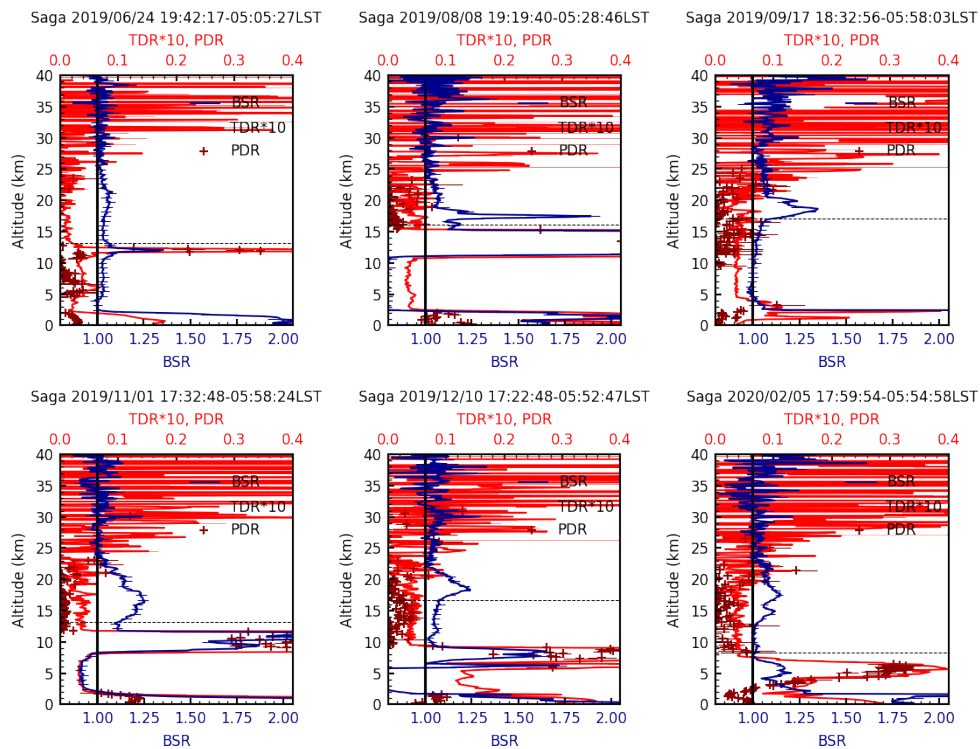


Fig. 3 Vertical profiles of aerosol backscattering ratio (*BSR*), total depolarization ratio (*TDR*), and particle depolarization ratio (*PDR*) at 532 nm over Saga, Japan, after the Raikoke volcanic eruption in June 2019. The horizontal dotted lines show the mean tropopause altitudes.

km on 8 August after the Raikoke eruption. The *BSR* peak of the background stratospheric aerosol layer composed of sulfuric acid particles mainly generated from carbonyl sulfide (COS) originating in the troposphere is around 20 km as shown on 24 June 2019. The *BSR* peak due to volcanic eruptions is approximately determined by the SO₂ injection altitude, i.e., the height of potential temperature. From September 2019 to February 2020, the *BSR* peak of the stratospheric aerosol layer was located around 18 km. Because the *PDR* was small, the particles were inferred to be sulfuric acid particles produced by chemical reaction of SO₂.

The Ulawun volcano in Papua New Guinea (5.05°S, 151.33°E) erupted on 26 June and 3 August 2019. The total mass of SO₂ from the two explosions was estimated to be 0.3 Tg. The Ulawun plume was transported mainly towards the south. Possible transport towards the north within the Brewer-Dobson Circulation was masked by already increased *sAOD* values from the Raikoke eruption in the Northern Hemisphere.²¹⁾ Lidar observations at Saga also did not clearly capture the impact of the Ulawun volcanic eruption.

3.3. Detection of smoke particles from large Canadian forest fires in summer 2017

Pyrocumulonimbus (pyroCb) from large forest fires can inject material containing smoke particles into the lower stratosphere, similar to volcanic explosions.²⁴⁾ The mass of smoke aerosol particles injected into the lower stratosphere from five near-simultaneous intense pyroCbs occurring in western North America on 12 August 2017 was comparable to that of a moderate volcanic eruption and an order of magnitude larger than previous benchmarks for extreme pyroCb activity.²⁵⁾

Extreme levels of Canadian wildfire smoke were observed in the stratosphere over central Europe on 21–22 August 2017 by European Aerosol Research Lidar Network (EARLINET) lidars.²⁶⁾ The smoke plume was also detected by lidar at Observatoire de Haute-Provence (43.9°N, 5.7°E) in France on 24 August as a 1-km-thick layer centered at 14.9 km; the peak *BSR* values were 8–10 around 19 km on 29 August.²⁷⁾ The first smoke layer was observed between 15.0 km and 15.8 km with the maximum *BSR* of 5.8 at 15.4 km over Tomsk (56.48°N, 85.05°E) in Russia on 26 August 2017.²⁸⁾

On 31 August 2017, an aerosol layer containing smoke particles with peak values of 2.0 for *BSR*, 0.08 for *TDR*, and 0.17 for *PDR* was observed at an altitude of 17.62 km over Saga (Fig. 4). The smoke layer rose to 20.31 km on 9 Octo-

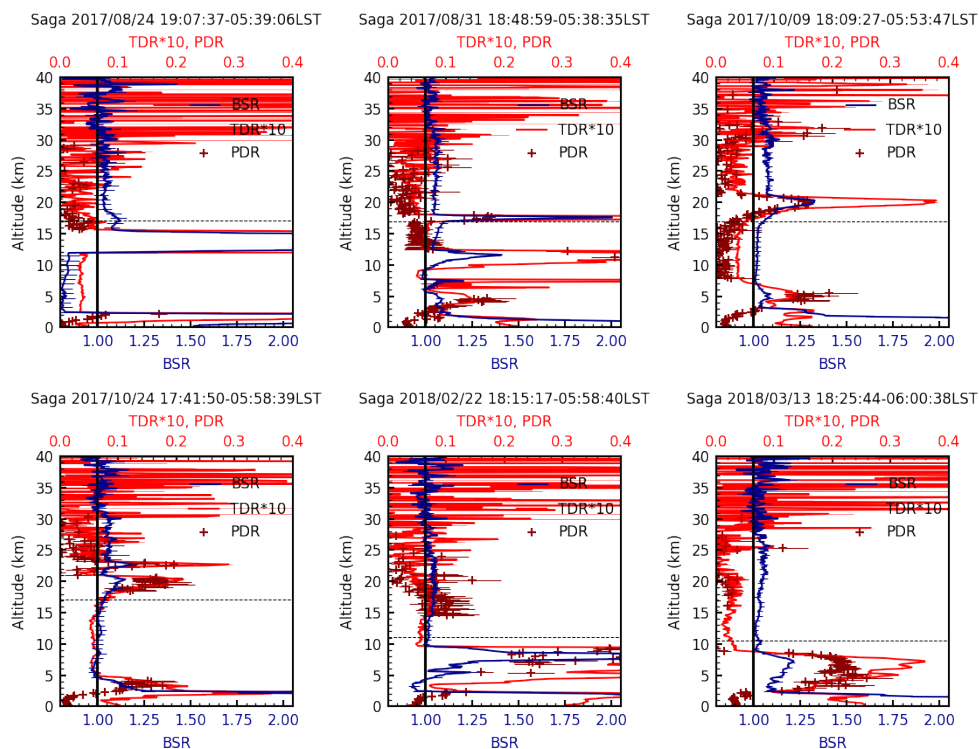


Fig. 4 Vertical profiles of aerosol backscattering ratio (*BSR*), total depolarization ratio (*TDR*), and particle depolarization ratio (*PDR*) at 532 nm over Saga, Japan, after Canadian forest fires in August 2017. The horizontal dotted lines show the mean tropopause altitudes.

ber 2017. Furthermore, on October 24, in addition to the layer near 20.31 km, a layer with a large *PDR* value was detected at 22.71 km. The smoke layer rose owing to solar heating of black carbon.²⁹⁾ High values of *PDR* (>0.1) were observed at an altitude of 16–20 km until February 2018.

A high particle depolarization ratio of 0.18 in a stratospheric layer from 15–16 km altitude and a small particle depolarization of 0.03 in a tropospheric layer at 5–6.5 km were observed at 532 nm by the Leipzig (51.3°N, 12.4°E) lidar system in Germany on 22 August 2017.³⁰⁾ A smoke *PDR* of 0.18–0.20 was observed at Lille (50.61°N, 3.14°E) in France in late August 2017.³¹⁾ These large *PDR* values would be expected to persist in the stratosphere because there is less water vapor in the stratosphere. Subsequently, smoke particles or aerosols mixed with smoke particles might have been transported to the troposphere in March 2018, because *PDR* values were small at ca. 20 km altitude on 13 March 2018 (Fig. 4).

4. Integrated backscattering coefficients of stratospheric aerosols

The temporal variation of the integrated backscattering coefficient (*IBC*) from tropopause to an altitude of 33 km and the tropopause altitude over Saga are shown in Fig. 5. In general, the tropopause altitude was low in winter to spring and high in summer. After the 2011 Nabro eruption and the 2019 Raikoke eruption, the *IBC* values clearly increased. The maximum *IBC* after the Nabro eruption was $3.65 \times 10^{-4} \text{ sr}^{-1}$ on 25 July 2011, and the maximum *IBC* after the Raikoke eruption was $3.01 \times 10^{-4} \text{ sr}^{-1}$ on 1 November 2019.

In our previous paper,⁵⁾ the maximum value of *IBC* was $4.19 \times 10^{-4} \text{ sr}^{-1}$ on 23 June 2011 after the Nabro eruption, whereas in this paper it was $3.65 \times 10^{-4} \text{ sr}^{-1}$ on 25 July 2011. The tropopause altitude on June 23 was 16.94 km from JRA-55, but it was 15.66 km from the radiosonde data of Fukuoka, near Saga, that was used in the previous paper. Calculating the *IBC* from 15.66 km to 33 km on June 23 gives a value of $3.93 \times 10^{-4} \text{ sr}^{-1}$, which might be the maximum value after the Nabro eruption. The tropopause altitude from JRA-55 data seems to be higher than that from radiosonde data. The difference between the *IBC* values of $4.19 \times 10^{-4} \text{ sr}^{-1}$ and $3.93 \times 10^{-4} \text{ sr}^{-1}$ is due to differences in normalization and integration time.

After the eruption of Kelud volcano (7.94°S, 112.31°E) on February 13, 2014, volcanic ash-containing aerosols with *BSRs* of 1.07 and 1.12 and *PDRs* of 0.05 and 0.08 were observed around 17 km altitude on April 10 and 12, respectively. The *IBC* values were $9.93 \times 10^{-5} \text{ sr}^{-1}$ and $1.09 \times 10^{-4} \text{ sr}^{-1}$, respectively, and there was no significant increase. The impact of Ambae (15.39°S, 167.84°E) eruption in April and July 2018 could not be detected at Saga.

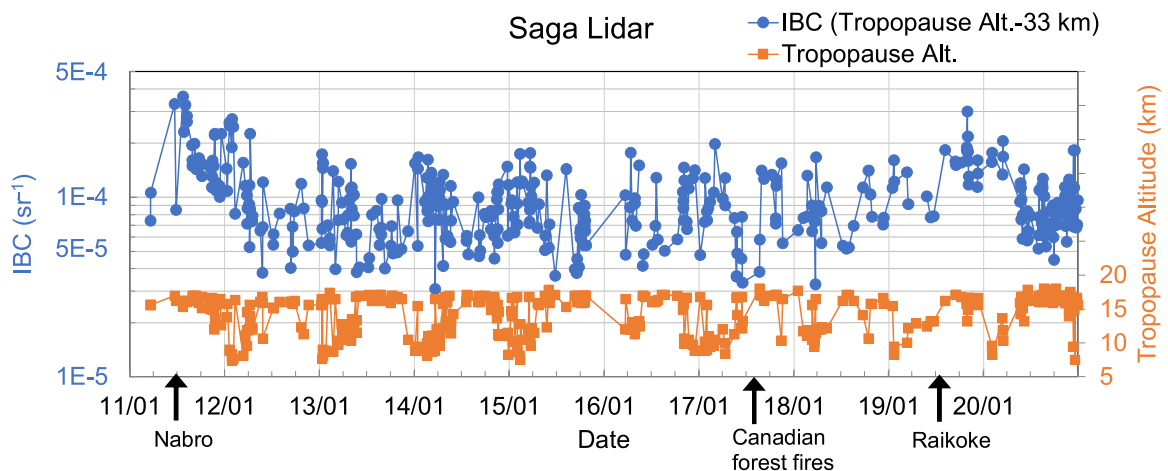


Fig. 5 Temporal variation of the integrated backscattering coefficient (*IBC*) from tropopause to an altitude of 33 km and tropopause altitude over Saga, Japan from 2011 to 2020. Arrows on the horizontal axis indicate the dates of volcanic eruptions and forest fires.

5. Discussion and concluding remarks

Lidar observations at Saga obtained over a 10-year period (2011–2020) demonstrated that stratospheric aerosols

increased after the June 2011 Nabro volcanic eruption and the June 2019 Raikoke volcanic eruption. The maximum values of *BSR* and *IBC* after the Nabro eruption were 3.70 at 18.22 km altitude on 23 June 2011 and $3.65 \times 10^{-4} \text{ sr}^{-1}$ on 25 July 2011, respectively; those after the Raikoke eruption were 1.89 at 17.47 km on 8 August 2019 and $3.01 \times 10^{-4} \text{ sr}^{-1}$ on 1 November 2019, respectively. Assuming a lidar ratio of 50 sr at 532 nm, the maximum stratospheric aerosol optical depth (*sAOD*) over Saga between 2011 and 2020 was estimated to be 0.018 on 25 July 2011. This *sAOD* is one-sixteenth of the maximum *sAOD* of 0.3 observed in February 1992 by the Tsukuba lidar after the Pinatubo eruption.³²⁾ The largest mean optical thickness of the Pinatubo-associated layer was 0.31 at 500 nm on 23 August 1991 in the latitude zone 20°S to 30°N,³³⁾ and monthly means of *sAOD* reached 0.2 in early 1992 at three lidar stations, Naha (26.2°N, 127.7°E) and Tsukuba in Japan and Garmisch-Partenkirchen (47.5°N, 11.1°E) in Germany.³⁴⁾ Although the *sAOD* of the stratospheric aerosols from the 2011 Nabro eruption was approximately 16 times smaller than the *sAOD* of the 1991 Pinatubo eruption, the resulting negative radiative forcing cannot be ignored, as discussed below.

The annual mean *IBC* value from 2013 to 2018, when stratospheric aerosols were considered normal, was $8.95 \times 10^{-5} \text{ sr}^{-1}$. The annual average *IBC* in 2011 after the Nabro eruption was $1.76 \times 10^{-4} \text{ sr}^{-1}$, $8.65 \times 10^{-5} \text{ sr}^{-1}$ higher than the annual mean. Converting these values to *sAOD* yields an increase of 0.0043. In addition, the *IBC* was $1.49 \times 10^{-4} \text{ sr}^{-1}$ in 2019 after the Raikoke eruption, $5.95 \times 10^{-5} \text{ sr}^{-1}$ larger than the 2013–2018 annual mean, and yielding an *sAOD* increase of 0.0030. The corresponding increases of negative radiative forcing in 2011 and 2019 were roughly 0.11 W m^{-2} and 0.07 W m^{-2} , respectively, based on a conversion factor from *sAOD* to radiative forcing of 25 W m^{-2} .^{35,36)} The increase in radiative forcing due to CO₂ from 2016 to 2017 was 0.028 W m^{-2} and the total radiative forcing due to all greenhouse gases was 0.034 W m^{-2} .³⁷⁾ Therefore, the temporary negative radiative forcing due to the increase in stratospheric aerosols after the Nabro and Raikoke volcanic eruptions might have exceeded the annual radiative forcing due to all greenhouse gases.

Stratospheric smoke particles from the 2017 Canadian forest fires were detected by the Saga lidar. The degree of depolarization of smoke particles was about 0.1–0.18, and this value persisted for a long period of time, from 31 August 2017 to 22 February 2018. As shown by the record-breaking wildfires in southeastern Australia in late December 2019 and early January 2020, global warming will increase the influx of smoke particles into the stratosphere due to pyroCb clouds.

Acknowledgements

Lidar operation at Saga is supported in part by the GOSAT series project. We would like to thank S. Takubo, T. Kawasaki, T. Akaho, S. Okano, G. Hamano, and H. Sakaguchi for their lidar observations. The world blank map in Fig. 1 was reproduced from <https://happylicilac.net/sy-sekaitizu-s3.html>.

References

- 1) M. P. McCormick, L. W. Thomason, and C. R. Trepte, "Atmospheric effects of Mt Pinatubo eruption," *Nature*, **373**, 399–404 (1995), <https://doi.org/10.1038/373399a0>.
- 2) S. Solomon, K. Dube, K. Stone, P. Yu, D. Kinnison, O. B. Toon, S. E. Strahan, K. H. Rosenlof, R. Portmann, S. Davis, W. Randel, P. Bernath, C. Boone, C. G. Bardeen, A. Bourassa, D. Zawada, and D. Degenstein, "On the stratospheric chemistry of midlatitude wildfire smoke," *Proc. Natl. Acad. Sci. USA.*, **119**, e2117325119, (2022), <https://doi.org/10.1073/pnas.2117325119>.
- 3) N. Trieu, I. Morino, O. Uchino, Y. Tsutsumi, T. Sakai, T. Nagai, A. Yamazaki, H. Okumura, K. Arai, K. Shiomi, D. F. Pollard, and B. Liley, "Influences of aerosols and thin cirrus clouds on GOSAT XCO₂ and XCH₄ using Total Carbon Column Observing Network, sky radiometer, and lidar data," *Int. J. Rem. Sens.*, **43**, 1770–1799 (2022), <https://doi.org/10.1080/01431161.2022.2038395>.
- 4) C. W. O'Dell, A. Eldering, P. O. Wennberg, D. Crisp, M. R. Gunson, B. Fisher, C. Frankenberg, M. Kiel, H. Lindqvist, L. Mandrake, A. Merrelli, V. Natraj, R. R. Nelson, G. B. Osterman, V. H. Payne, T. E. Taylor, D. Wunch, B. J. Drouin, F. Oiyafuso, A. Chang, J. McDuffie, M. Smyth, D. F. Baker, S. Basu, F. Chevallier, S. M. R. Crowell, L. Feng, P. I. Palmer, M. Dubey, O. E. García, D. W. T. Griffith, F. Hase, L. T. Iraci, R. Kivi, I. Morino, J. Notholt, H. Ohyama, C. Petri, C. M. Roehl, M. K. Sha, K. Strong, R. Sussmann, Y. Te, O. Uchino, and V. A. Velazco, "Improved retrievals of carbon dioxide from Orbiting Carbon Observatory-2 with the version 8 ACOS algorithm," *Atmos. Meas. Tech.*, **11**, 6539–6576 (2018), <https://doi.org/10.5194/amt-11-6539-2018>.

- org/10.5194/amt-11-6539-2018.
- 5) O. Uchino, T. Sakai, T. Nagai, K. Nakamae, I. Morino, K. Arai, H. Okumura, S. Takubo, T. Kawasaki, Y. Mano, T. Matsunaga, and T. Yokota, "On recent (2008–2012) stratospheric aerosols observed by lidar over Japan," *Atmos. Chem. Phys.*, **12**, 11975–11984 (2012), <https://doi.org/10.5194/acp-12-11975-2012>.
 - 6) O. Uchino, T. Sakai, T. Izumi, T. Nagai, I. Morino, A. Yamazaki, M. Deushi, K. Yumimoto, K., T. Maki, T. Y. Tanaka, T. Akaho, H. Okumura, K. Arai, T. Nakatsuru, T. Matsunaga, and T. Yokota, "Lidar detection of high concentrations of ozone and aerosol transported from northeastern Asia over Saga, Japan," *Atmos. Chem. Phys.*, **17**, 1865–1879 (2017), <https://doi.org/10.5194/acp-17-1865-2017>.
 - 7) S. Kobayashi, Y. Ota, Y. Harada, A. Ebita, M. Moriya, H. Onoda, K. Onogi, H. Kamahori, C. Kobayashi, H. Endo, K. Miyaoka, and K. Takahashi, "The JRA-55 Reanalysis: General specifications and basic characteristics," *J. Meteor. Soc. Japan*, **93**, 5–48 (2015), <https://doi.org/10.2151/jmsj.2015-001>.
 - 8) WOUDC - World Ozone and Ultraviolet Radiation Data Centre, <https://woudc.org/home.php> (Accessed 2023.10.11)
 - 9) H. Jäger and T. Deshler, "Correction to "Lidar backscatter to extinction, mass and area conversions for stratospheric aerosols based on midlatitude balloonborne size distribution measurements"," *Geophys. Res. Lett.*, **30**(7), 1382 (2003), <https://doi.org/10.1029/2003GL017189>.
 - 10) J.-P. Vernier, J. P. Pommereau, A. Garnier, J. Pelon, N. Larsen, J. Nielsen, T. Christiansen, F. Cairo, L. W. Thomason, T. Leblanc, and I. S. McDermid, "Tropical stratospheric aerosol layer from CALIPSO lidar observations," *J. Geophys. Res.*, **114**, D00H10 (2009), <https://doi.org/10.1029/2009JD011946>.
 - 11) J. Kar, M. A. Vaughan, K.-P. Lee, J. L. Tackett, M. A. Avery, A. Garnier, B. J. Getzewich, W. H. Hunt, D. Josset, Z. Liu, P. L. Lucker, B. Magill, A. H. Omar, J. Pelon, R. R. Rogers, T. D. Toth, C. R. Trepte, J.-P. Vernier, D. M. Winker, and S. A. Young, "CALIPSO lidar calibration at 532 nm: version 4 nighttime algorithm," *Atmos. Meas. Tech.*, **11**, 1459–1479 (2018), <https://doi.org/10.5194/amt-11-1459-2018>.
 - 12) J. Kar, K.-P. Lee, M. A. Vaughan, J. L. Tackett, C. R. Trepte, D. M. Winker, P. L. Lucker, and B. J. Getzewich, "CALIPSO level 3 stratospheric aerosol profile product: version 1.00 algorithm description and initial assessment," *Atmos. Meas. Tech.*, **12**, 6173–6191 (2019), <https://doi.org/10.5194/amt-12-6173-2019>.
 - 13) F. G. Fernald, "Analysis of atmospheric lidar observations: some comments," *Appl. Opt.*, **23**, 652–653 (1984), <https://doi.org/10.1364/AO.23.000652>.
 - 14) V. Freudenthaler, M. Esselborn, M. Wiegner, B. Heese, M. Tesche, A. Ansmann, D. Müller, D. Althausen, M. Wirth, A. Fix, G. Ehret, P. Knippertz, C. Toledano, J. Gasteiger, M. Garhammer, and M. Seefeldner, "Depolarization ratio profiling at several wavelengths in pure Saharan dust during SAMUM 2006," *Tellus B*, **61**, 165–179 (2009), <https://doi.org/10.1111/j.1600-0889.2008.00396.x>.
 - 15) A. Behrendt and T. Nakamura, "Calculation of the calibration constant of polarization lidar and its dependency on atmospheric temperature," *Opt. Express*, **10**, 805–817 (2002).
 - 16) L. Clarisse, D. Hurtmans, C. Clerbaux, J. Hadji-Lazaro, Y. Ngadi, and P.-F. Coheur, "Retrieval of sulphur dioxide from the infrared atmospheric sounding interferometer (IASI)," *Atmos. Meas. Tech.*, **5**, 581–594 (2012), <https://doi.org/10.5194/amt-5-581-2012>.
 - 17) T. Sakai, O. Uchino, T. Nagai, B. Liley, I. Morino, and T. Fujimoto, "Long-term variation of stratospheric aerosols observed with lidars over Tsukuba, Japan, from 1982 and Lauder, New Zealand, from 1992 to 2015," *J. Geophys. Res.-Atmos.*, **121**, 10283–10293 (2016), <https://doi.org/10.1002/2016JD025132>.
 - 18) L. O. Muser, G. A. Hoshyaripour, J. Bruckert, Á. Horváth, E. Malinina, S. Wallis, F. J. Prata, A. Rozanov, C. von Savigny, H. Vogel, and B. Vogel, "Particle aging and aerosol-radiation interaction affect volcanic plume dispersion: evidence from the Raikoke 2019 eruption," *Atmos. Chem. Phys.*, **20**, 15015–15036 (2020), <https://doi.org/10.5194/acp-20-15015-2020>.
 - 19) J. de Leeuw, A. Schmidt, C. S. Witham, N. Theys, I. A. Taylor, R. G. Grainger, R. J. Pope, J. Haywood, M. Osborne, and N. I. Kristiansen, "The 2019 Raikoke volcanic eruption-Part 1: Dispersion model simulations and satellite retrievals of volcanic sulfur dioxide," *Atmos. Chem. Phys.*, **21**, 10851–10879 (2021), <https://doi.org/10.5194/acp-21-10851-2021>.
 - 20) Z. Cai, S. Griessbach, and L. Hoffmann, "Improved estimation of volcanic SO₂ injections from satellite retrievals and Lagrangian transport simulations: the 2019 Raikoke eruption," *Atmos. Chem. Phys.*, **22**, 6787–6809 (2022), <https://doi.org/10.5194/acp-22-6787-2022>.
 - 21) C. Kloss, G. Berthet, P. Sellitto, F. Ploeger, G. Taha, M. Tidiga, M. Eremenko, A. Bossolasco, F. Jégou, J.-B. Renard, and B. Legras, "Stratospheric aerosol layer perturbation caused by the 2019 Raikoke and Ulawun eruptions and their radiative forcing," *Atmos. Chem. Phys.*, **21**, 535–560 (2021), <https://doi.org/10.5194/acp-21-535-2021>.
 - 22) G. Vaughan, D. Wareing, and H. Ricketts, "Measurement Report: Lidar measurements of stratospheric aerosol following the 2019 Raikoke and Ulawun volcanic eruptions," *Atmos. Chem. Phys.*, **21**, 5597–5604 (2021), <https://doi.org/10.5194/acp-21-5597-2021>.
 - 23) F. Chouza, T. Leblanc, J. Barnes, M. Brewer, P. Wang, and D. Koon, "Long-term (1999–2019) variability of stratospheric

- aerosol over Mauna Loa, Hawaii, as seen by two co-located lidars and satellite measurements,” *Atmos. Chem. Phys.*, **20**, 6821–6839 (2020), <https://doi.org/10.5194/acp-20-6821-2020>.
- 24) M. Fromm, R. Bevilacqua, R. Servranckx, J. Rosen, J. P. Thayer, J. Herman, and D. Larko, “Pyro-cumulonimbus injection of smoke to the stratosphere: Observations and impact of a super blowup in northwestern Canada on 3–4 August 1998,” *J. Geophys. Res.-Atmos.*, **110**, D08205 (2005), <https://doi.org/10.1029/2004JD005350>.
 - 25) D. A. Peterson, J. R. Campbell, E. J. Hyer, M. D. Fromm, G. P. Kablick, J. H. Cossuth, and M. T. DeLand, “Wildfire-driven thunderstorms cause a volcano-like stratospheric injection of smoke,” *npj Clim. Atmos. Sci.*, **1**, 30 (2018), <https://doi.org/10.1038/s41612-018-0039-3>.
 - 26) A. Ansmann, H. Baars, A. Chudnovsky, I. Mattis, I. Veselovskii, M. Haarig, P. Seifert, R. Engelmann, and U. Wandinger, “Extreme levels of Canadian wildfire smoke in the stratosphere over central Europe on 21–22 August 2017,” *Atmos. Chem. Phys.*, **18**, 11831–11845 (2018), <https://doi.org/10.5194/acp-18-11831-2018>.
 - 27) S. M. Khaykin, S. Godin-Beekmann, A. Hauchecorne, J. Pelon, F. Ravetta, and P. Keckut, “Stratospheric smoke with unprecedentedly high backscatter observed by lidars above southern France,” *Geophys. Res. Lett.*, **45**, 1639–1646 (2018), <https://doi.org/10.1002/2017GL076763>.
 - 28) V. V. Zuev, V. V. Gerasimov, A. V. Nevzorov, and E. S. Savelieva, “Lidar observations of pyrocumulonimbus smoke plumes in the UTLS over Tomsk (Western Siberia, Russia) from 2000 to 2017,” *Atmos. Chem. Phys.*, **19**, 3341–3356 (2019), <https://doi.org/10.5194/acp-19-3341-2019>.
 - 29) P. Yu, O. B. Toon, C. G. Bardeen, Y. Zhu, K. H. Rosenlof, R. W. Portmann, T. D. Thornberry, R. S. Gao, S. M. Davis, E. T. Wolf, J. de Gouw, D. A. Peterson, M. D. Fromm, and A. Robock, “Black carbon lofts wildfire smoke high into the stratosphere to form a persistent plume,” *Science*, **365**, 587–590 (2019), <https://doi.org/10.1126/science.aax1748>.
 - 30) M. Haarig, A. Ansmann, H. Baars, C. Jimenez, I. Veselovskii, R. Ronny Engelmann, and D. Althausen, “Depolarization and lidar ratios at 355, 532, and 1064 nm and microphysical properties of aged tropospheric and stratospheric Canadian wildfire smoke,” *Atmos. Chem. Phys.*, **18**, 11847–11861 (2018), <https://doi.org/10.5194/acp-18-11847-2018>.
 - 31) Q. Hu, P. Goloub, I. Veselovskii, J.-A. Bravo-Aranda, I. E. Popovici, T. Podvin, M. Haeffelin, A. Lopatin, O. Dubovik, C. Pietras, X. Huang, B. Torres, and C. Chen, “Long-range transported Canadian smoke plumes in the lower stratosphere over northern France,” *Atmos. Chem. Phys.*, **19**, 1173–1193 (2019), <https://doi.org/10.5194/acp-19-1173-2019>.
 - 32) O. Uchino, “Scientific results of the EPIC projects,” *NATO ASI Ser.*, **142**, 127–139 (1996).
 - 33) L. L. Stowe, L. L. Carey, and P. P. Pellegrino, “Monitoring the Mt. Pinatubo aerosol layer with NOAA/11 AVHRR data,” *Geophys. Res. Lett.*, **19**, 159–162 (1992), <https://doi.org/10.1029/91GL02958>.
 - 34) H. Jäger, O. Uchino, T. Nagai, T. Fujimoto, V. Freudenthaler, and F. Homburg, “Ground-based remote sensing of the decay of the Pinatubo eruption cloud at three Northern Hemisphere sites,” *Geophys. Res. Lett.*, **22**, 607–610 (1995), <https://doi.org/10.1029/95GL00054>.
 - 35) J. Hansen, M. Sato, R. Ruedy, L. Nazarenko, A. Lacis, G. A. Schmidt, G. Russell, I. Aleinov, M. Bauer, S. Bauer, N. Bell, B. Cairns, V. Canuto, M. Chandler, Y. Cheng, A. Del Genio, G. Faluvegi, E. Fleming, A. Friend, T. Hall, C. Jackman, M. Kelley, N. Kiang, D. Koch, J. Lean, J. Lerner, K. Lo, S. Menon, R. Miller, P. Minnis, T. Novakov, V. Oinas, J. Perlwitz, J. Perlwitz, D. Rind, A. Romanou, D. Shindell, P. Stone, S. Sun, N. Tausnev, D. Thresher, B. Wielicki, T. Wong, M. Yao, and S. Zhang, “Efficacy of climate forcings,” *J. Geophys. Res.*, **110**, D18104 (2005), <https://doi.org/10.1029/2005JD005776>.
 - 36) S. Solomon, J. S. Daniel, R. R. Neely III, J.-P. Vernier, E. G. Dutton, and L. W. Thomason, “The persistently variable “background” stratospheric aerosol layer and global climate change,” *Science*, **333**, 866–870 (2011), <https://doi.org/10.1126/science.1206027>.
 - 37) NOAA, “The NOAA Annual Greenhouse Gas Index (AGGI),” <https://gml.noaa.gov/aggi/aggi.html> (Accessed 2023.10.11).

Author Introduction

Corresponding author: Osamu Uchino

Doctor of Science, Kyushu University, Fukuoka, Japan. Visiting researcher at the Meteorological Research Institute.